



CHORUS

This is the accepted manuscript made available via CHORUS. The article has been published as:

Driving missing data at next-to-leading order

Z. Bern, G. Diana, L. J. Dixon, F. Febres Cordero, S. Höche, H. Ita, D. A. Kosower, D. Maître,
and K. J. Ozeren

Phys. Rev. D **84**, 114002 — Published 2 December 2011

DOI: [10.1103/PhysRevD.84.114002](https://doi.org/10.1103/PhysRevD.84.114002)

Driving Missing Data at Next-to-Leading Order

Z. Bern^a, G. Diana^b, L. J. Dixon^{c,d}, F. Febres Cordero^e, S. Höche^d,
H. Ita^a, D. A. Kosower^b, D. Maître^{c,f} and K. J. Ozeren^a

^a*Department of Physics and Astronomy, UCLA, Los Angeles, CA 90095-1547, USA*

^b*Institut de Physique Théorique, CEA-Saclay, F-91191 Gif-sur-Yvette cedex, France*

^c*Theory Division, Physics Department, CERN, CH-1211 Geneva 23, Switzerland*

^d*SLAC National Accelerator Laboratory, Stanford University, Stanford, CA 94309, USA*

^e*Departamento de Física, Universidad Simón Bolívar, Caracas 1080A, Venezuela*

^f*Department of Physics, University of Durham, Durham DH1 3LE, UK*

Abstract

The prediction of backgrounds to new physics signals in topologies with large missing transverse energy and jets is important to new physics searches at the LHC. Following a CMS study, we investigate theoretical issues in using measurements of $\gamma + 2$ -jet production to predict the irreducible background to searches for missing energy plus two jets that originates from $Z + 2$ -jet production where the Z boson decays to neutrinos. We compute ratios of $\gamma + 2$ -jet to $Z + 2$ -jet production cross sections and kinematic distributions at next-to-leading order in α_s , as well as using a parton shower matched to leading-order matrix elements. The former ratios rely on the first next-to-leading order calculation of $\gamma + 2$ -jet production at a hadron collider. We find that the ratios obtained in the two approximations are quite similar, making $\gamma + 2$ -jet production a theoretically reliable estimator for the missing energy plus two jets background. We employ a Frixione-style photon isolation, but we also show that for isolated prompt photon production at high transverse momentum the difference between this criterion and the standard cone isolation used by CMS is small.

PACS numbers: 12.38.Bx, 13.85.Qk, 13.87.Ce

I. INTRODUCTION

The LHC era is now upon us, and the hunt for the mechanism of electroweak symmetry breaking and new physics beyond the standard model is underway. Typical signatures for supersymmetry and many other new physics models include topologies with large missing transverse energy (MET) accompanying jets (METJ). The same signatures can easily be mimicked by Standard Model processes, such as the production of an electroweak boson decaying into neutrinos, in association with jets. For the discovery of new physics in the early running of the LHC, with only a few inverse femtobarns of integrated luminosity, it is important to understand the Standard Model backgrounds to METJ searches.

Events containing a Z boson and jets, with the Z decaying into a neutrino pair (METZJ), constitute an irreducible background to the METJ signal. One can envisage using complementary approaches to understanding this and other backgrounds: a direct theoretical prediction; or data-driven approaches, which estimate the rate from measurements of other processes (or possibly from other kinematic regions in the same process). Data-driven techniques offer a powerful means of avoiding theoretical uncertainties in background predictions, as well as cancelling experimental systematics common to different processes. However, such methods can require theoretical assistance, in order to estimate the “translation” parameters from one process to another, and their inherent uncertainties. The question theorists can address is how stable is the ratio of two processes to various theoretical approximations.

In the case of the process $Z(\rightarrow \nu\bar{\nu}) + \text{jets}$, the most obvious choice of other process would be $Z(\rightarrow \ell^+\ell^-) + \text{jets}$, *i.e.* the production of a Z boson in association with jets, where the Z decays into a charged lepton pair. The production kinematics and dynamics of these two processes are identical, so no theoretical input about QCD is required, only knowledge of the Z boson branching ratios. Leptonically decaying Z bosons have the drawback, however, of offering very low event rates, less than a sixth of METZJ (per lepton channel), even before imposing lepton rapidity cuts. The paucity of statistics has led experimenters to examine using other processes to estimate METZJ rates and distributions. The CMS collaboration has studied [1, 2] the use of W or photon production in association with jets for estimating the METZJ background. The production of a W in association with jets offers an order of magnitude higher statistics than the leptonic Z process; the production of a prompt photon in association with jets, sixteenfold higher statistics than leptonic Z decays. In addition,

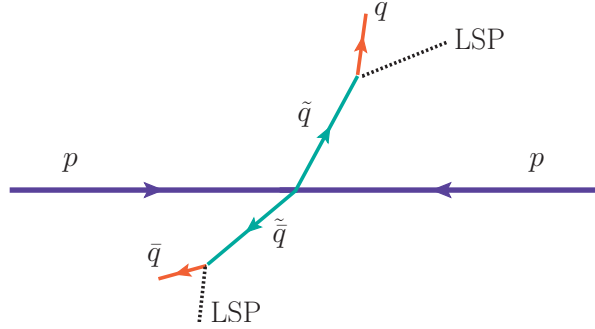


FIG. 1: Squark pair production illustrates a new physics process with the signature of two jets plus MET. Here each squarks decays to a quark and the lightest neutralino; the escaping neutralinos generate the missing transverse energy.

W production suffers from contamination from $t\bar{t}$ events, and could well be affected by the same kinds of new physics the experiments are seeking in the METZJ sample. Reducing $t\bar{t}$ contamination requires selection cuts that enhance the photon channel’s advantage.

Use of either the W or γ plus jets processes requires knowledge of their short-distance strong-interaction dynamics, as they probe different combinations of the parton distributions and somewhat different scales than Z plus jets. In the photon case, its masslessness also affects distributions in important ways and requires theoretical input for any comparison with massive boson production. The study of both processes is valuable, of course; the use of different processes allows for cross checks and also presumably different sensitivity to whatever new physics may be lurking in the data.

In this paper, we study the $\gamma + 2$ -jet and $Z(\rightarrow \nu\bar{\nu}) + 2$ -jet production processes. The latter process is a background to new physics, such as the squark pair-production process illustrated in fig. 1. Our aim is to provide the necessary theoretical results, to next-to-leading order (NLO) accuracy in the strong coupling α_s , for using $\gamma + 2$ -jet production to estimate $Z + 2$ -jet production. In particular, we provide an estimate of the theoretical uncertainties that enter the recent new physics search performed by CMS using a signature of three jets and large missing transverse momentum [36]. Our paper also represents the first computation of the NLO QCD corrections to $\gamma + 2$ -jet production at a hadron collider. We use the same software tools as in our previous studies of $W + n$ - and $Z + n$ -jet production [3–6], the BLACKHAT library [7, 8] along with AMEGIC++ [9] within the SHERPA [10]

framework, to perform the leading-order (LO) and NLO calculations. We also present results for a parton-shower calculation matched to fixed-order LO matrix elements (ME+PS) [11], also within the SHERPA [10] framework. A key issue is the theoretical uncertainty in the conversion from γ to Z . We use the difference between the ME+PS results and the NLO predictions to estimate the uncertainties for ratios. (The common variation of factorization and renormalization scales in the numerator and denominator of these ratios produces quite small shifts in the ratios, which are likely to underestimate the uncertainties substantially.) The results presented here are being used by the CMS collaboration in their study of missing energy in association with three jets [2]. While our present study is for missing energy in association with two jets, we do not expect much difference in the theoretical uncertainties between the two- and three-jet cases.

Photon isolation is essential for rejecting copious hadronic backgrounds. The type of photon isolation criterion affects the theoretical description of the photon production process. In the past, various types of isolation cones have been used, which limit the amount of hadronic energy near the photon candidate. Fixed isolation cones generally limit the total amount of energy in a cone, while the one proposed by Frixione [12] consists of a set of energy constraints that become increasingly restrictive the closer one gets to the photon. The Frixione cone is theoretically attractive because it eliminates contributions from long-distance collinear fragmentation of partons into photons. Although there is a perturbative factorization available for other types of cones, the required photon fragmentation functions [13] (non-perturbative functions analogous to the parton distribution functions) are not known particularly precisely. From an experimental point of view, some hadronic energy must be allowed everywhere within the cone in order to cope with the underlying event and with event pile-up. In our study, we adopt a modified cone criterion of the Frixione type. The CMS collaboration has recently published [14] a measurement of the photon spectrum. We compare the two types of cone isolation to the data, and show that with our choice of parameters the difference between them is small for the kinematic region studied by CMS.

In the following section we describe the details of our calculation and discuss the photon isolation criterion. Section III presents our cross-check using isolated prompt-photon production. Section IV discusses the cuts we use. In section V we present the ratios of $Z + 2$ -jet to $\gamma + 2$ -jet rates for a variety of distributions. Our conclusions and outlook follow.

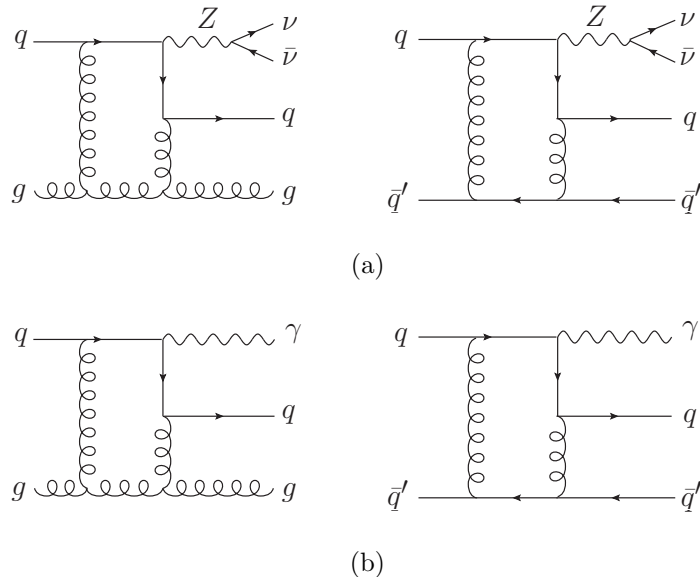


FIG. 2: Sample virtual diagrams needed for (a) $pp \rightarrow Z(\rightarrow \nu\bar{\nu}) + 2\text{-jet}$ production and for (b) $pp \rightarrow \gamma + 2\text{-jet}$ production.

II. THE CALCULATION

In this section we discuss our calculational setup. At NLO, we follow the same basic setup used in refs. [3–5] while for the ME+PS study we use the setup of ref. [11].

A. Matrix Elements and Integration

We compute the cross sections at NLO using the Catani–Seymour dipole subtraction method [15]. This method requires the combination of several contributions: the LO term; virtual corrections from the interference of tree-level and one-loop amplitudes; the real-emission corrections with dipole subtraction terms; and the singular phase-space integrals of the dipole terms.

We evaluate the required one-loop amplitudes using the BLACKHAT program library [7]. For the processes we are studying, we need the one-loop corrections to the following partonic processes,

$$\begin{aligned}
 q\bar{q}gg &\rightarrow Z(\rightarrow \nu\bar{\nu}) \text{ or } \gamma, \\
 q\bar{q}q'\bar{q}' &\rightarrow Z(\rightarrow \nu\bar{\nu}) \text{ or } \gamma,
 \end{aligned}
 \tag{2.1}$$

where two of the four partons should be crossed into the final state, and the Z decay to neutrinos is folded in. Some sample diagrams for these processes are shown in fig. 2, illustrating the similarity of the Z and γ cases.

For the Z processes, the BLACKHAT code library [7, 8] implements analytic one-loop amplitudes from refs. [16, 17]. (See also ref. [18].) The photonic amplitudes are implemented using analytic formulæ in a similar way; they can be obtained as appropriate sums of color-ordered primitive amplitudes for the two-quark three-gluon [19] and four-quark one-gluon processes [20], as explained in ref. [21] and in the fourth appendix of ref. [19]. This conversion is possible because the trace-based color decomposition does not distinguish between different generators of $U(N)$. Setting one of the generators equal to the identity matrix, and collecting the coefficients of the identical remaining color structures, generates the photonic amplitudes. This procedure removes the unwanted three-boson couplings of the photon present in each primitive amplitude. We omit the process $gg \rightarrow gg\gamma$ as it only contributes to $\gamma + 2$ -jet production at next-to-next-to-leading order; for the kinematics of interest here the gluon luminosity is not large enough for this process to be important.

The NLO result also requires real-emission corrections to the LO process, which arise from tree-level amplitudes with one additional parton. We use the program AMEGIC++ [9] to compute these contributions, along with the Catani-Seymour dipole subtraction terms [15] and their integrals over phase space. The SHERPA framework [10] includes AMEGIC++ and tools to analyze the results and construct a wide variety of distributions. We have previously validated [3] the BLACKHAT+SHERPA framework for $W + (n \leq 2)$ jets against the MCFM code [22].

We use SHERPA in a second mode, to provide a parton-shower prediction matched to tree-level matrix elements (ME+PS), also known as matrix-element-plus-truncated-shower. (Our parton-shower results do not include hadronization effects, but remain at the parton level.) The ME+PS event samples are produced following ref. [11], using the COMIX matrix-element generator [23]. This method combines LO hard matrix elements together with parton showers, which resum logarithmic corrections due to Bremsstrahlung effects. The parton shower employed to this end in SHERPA [24] is based on Catani-Seymour dipole factorization [15]. In contrast to earlier parton showers, the procedure inherently respects QCD soft color coherence. The procedure allows the unambiguous identification of a recoil partner for partons that are shifted off mass-shell in the splitting process (the

“mother” partons). This eliminates one of the major sources of uncertainty in earlier schemes for parton evolution. As the observables presented below should be relatively insensitive to hadronization effects, ME+PS results are presented at the parton level. We match to matrix elements containing up to three final-state partons, and use 15 GeV for the merging cut. (Further details may be found in ref. [25].)

We work to leading order in the electroweak coupling. The Z -boson couplings are as given in ref. [5]. In particular, the $\nu\bar{\nu}$ invariant mass is distributed in a relativistic Breit-Wigner of width $\Gamma_Z = 2.49$ GeV about the Z boson mass of 91.1876 GeV. These values, along with those of $\alpha_{\text{QED}}(M_Z) = 1/128.802$ and $\sin^2\theta_W = 0.230$ lead to a branching ratio for the neutrino mode in Z decay of $\text{Br}(Z \rightarrow \nu\bar{\nu}) = 0.2007$. We use MSTW2008 leading and next-to-leading order parton distribution functions, with the QCD coupling α_s chosen appropriately in each case. Our LHC results are for a center-of-mass energy of 7 TeV.

The question of what scale should be chosen for the electromagnetic coupling in a prompt-photon calculation is a subtle one. Strictly speaking, this scale is undetermined in a leading-order computation; and although we are working to NLO in the QCD coupling, we are only working to LO in the electromagnetic one. From a practical point of view, however, it makes a difference whether we choose a scale of order the photon transverse momentum (and hence $\alpha_{\text{EM}} \approx \alpha_{\text{EM}}(M_Z) \approx 1/128$), or the zero-momentum-squared value (that is, $\alpha_{\text{EM}}(0) = 1/137.036$).

Heuristically, we see that the sequence of fermion bubbles on the photon forms a gauge-invariant set. Moreover, because of QED Ward identities, this is the only set of diagrams which controls the coupling renormalization. In the idealized situation we are considering, the photon is always resolved, *i.e.* it is not allowed to split into low-mass lepton pairs. Then summing the bubbles leads to a zero-momentum-squared coupling for the emission of the hard photon. Other types of QED effects, such as emission of additional hard photons, change the kinematics and cannot be absorbed into a running coupling. This argument is confirmed by the analyses in refs. [26, 27]. We therefore take the electromagnetic coupling for the prompt-photon computation to be the zero-momentum-squared value, $\alpha_{\text{EM}}(0) = 1/137.036$, and *not* the running value at typical collider energies.

B. Infrared Safety and Photon Isolation

An observable in perturbative QCD is infrared- and collinear-safe if it is unaltered under the emission of an arbitrarily soft gluon, or the splitting of a colored parton into a pair of colored partons (whether in the initial or final state). We follow ATLAS and CMS in using the infrared-safe anti- k_T jet algorithm [28].

For $\gamma + 2$ -jet production, there is an additional infrared issue beyond the infrared safety of the jet algorithm. Because photons can arise from π^0 decay and other hadronic sources, it is essential from an experimental point of view to insist that they be isolated from jets if we want to study photons that originate in short-distance physics (‘prompt’). On the other hand, too strict a photon isolation criterion — such as requiring no hadrons or no hadronic energy in a cone around the photon, or using tracking alone to determine isolation — would be infrared-unsafe, and prevent the use of perturbative QCD as a theoretical tool. In order to navigate between these two competing requirements, experimental collaborations typically use a weighted isolation criterion, imposing a limit on the hadronic energy fraction in a cone around the photon, or simply on the total hadronic energy in the cone.

In their recent measurement of the inclusive isolated prompt-photon spectrum [14], the CMS collaboration required photon candidates to satisfy a set of requirements on nearby energy deposits measured via tracking, and in the electromagnetic and hadronic calorimeters. In their theoretical modeling using PYTHIA, they required photons to have less than 5 GeV of summed p_T within an isolation cone of radius $R = 0.4$, where $R_{i\gamma} = \sqrt{(\eta_i - \eta_\gamma)^2 + (\phi_i - \phi_\gamma)^2}$. We will adopt this criterion as our ‘reference’ standard cone isolation in our discussion of the isolated prompt-photon spectrum.

While such a criterion is infrared-safe with respect to the strong interactions — emission of a soft gluon, or a colored parton splitting into two colored partons — it is *not* collinear-safe with respect to QED: the cross-section receives contributions from collinear radiation of photons off massless quarks. In a theoretical description, this singularity has to be factorized, and absorbed into parton-to-photon fragmentation functions [13], whose computation from first principles would require knowledge of non-perturbative physics. The factorization and the non-perturbative functions are the final-state analogs of the parton distribution functions. In practice, these functions are extracted from fits to experimental data, although these fits are not nearly as precise as those for the parton distributions,

nor are sets surrounding a central fit available to estimate errors. (As is true for the parton distributions, the evolution of the fragmentation function with the hard scale can be determined in perturbative QCD.)

However, the isolation criterion given above is not the only possible one. Frixione [12] proposed a modified isolation requirement which suppresses the collinear region of the phase space and thereby eliminates the need for a fragmentation-function contribution. We follow this proposal, requiring that each parton i within a distance $R_{i\gamma}$ of the photon obey

$$\sum_i E_{iT} \Theta(\delta - R_{i\gamma}) \leq \mathcal{H}(\delta), \quad (2.2)$$

for all $\delta \leq \delta_0$, in a cone of fixed half-angle δ_0 around the photon axis. The restricting function $\mathcal{H}(\delta)$ is chosen such that it vanishes as $\delta \rightarrow 0$ and thus suppresses collinear configurations, but allows soft radiation arbitrarily close to the photon. We adopt

$$\mathcal{H}(\delta) = E_T^\gamma \epsilon \left(\frac{1 - \cos \delta}{1 - \cos \delta_0} \right)^n, \quad (2.3)$$

where E_T^γ is the photon transverse energy.

An experimental analysis cannot adopt the Frixione prescription precisely, because of the finite resolution of detectors. One can imagine using a discretized version of it; this would still require a fragmentation contribution (corresponding to the innermost step of the discretized cone), but it would presumably have a much smaller one than the standard cone. One could imagine adjusting the parameters ϵ , δ_0 and n so as to minimize that contribution. A preliminary study of the comparison between the Frixione prescription and a discretized version may be found in ref. [29].

In our study, we will use the Frixione cone, with $\epsilon = 0.025$, $\delta_0 = 0.3$ and $n = 2$. In practice, we find that our predictions are only weakly sensitive to these parameters. In the next section, we will compare our predictions using these parameters to predictions made using a standard cone for the isolated prompt-photon spectrum [14] measured by CMS. As we shall see, the differences between the Frixione and standard-cone isolation prescriptions are not large, and are quite small in the large- p_T^γ region that is of primary interest in the present study. We therefore conclude that it is reasonable to use the Frixione isolation to model the Z -to-photon ratio in association with two jets for CMS's analysis.

In the definition of the cross section for $\gamma + m$ jets, at least m jets must lie outside the isolation cone, while we allow any number of additional jets m' to fall inside the cone of

radius $\delta_0 = 0.3$. In order to obtain the desired observable we apply the jet-finding algorithm to all partons except the photon in the event, to obtain m jets outside the isolation cone and m' jets inside the cone. Then we apply the cuts on transverse momenta and rapidity of the m jets. This procedure is infrared safe because the jet-finding algorithm is applied everywhere and not just outside the isolation cone. In practice, jets appear very rarely inside the photon isolation cone, because of the combination of the jet p_T cut and the small energy fraction we use. We will list the other cuts we apply in a later section.

III. ISOLATED PROMPT-PHOTON PRODUCTION

Recently, CMS has published a measurement [14] of the inclusive isolated prompt-photon spectrum based on a data sample of 2.9 pb^{-1} from early running of the LHC. They compared the measurement with NLO predictions from the publicly-available JETPHOX code [30]. These predictions make use of a standard photon isolation cone as described in the previous section, and include fragmentation contributions. (The JETPHOX code implements a Frixione isolation cone as well as a standard isolation cone, although the former implementation is not used in this study.) We can use the CMS study to assess the expected differences between the use of standard-cone isolation and a Frixione isolation for the photon. To do so, we have made use of an NLO code, due to Gordon and Vogelsang [31]. It is a semi-analytic code, relying on the narrow-cone approximation. We also used BLACKHAT in conjunction with SHERPA as a cross check on the NLO Frixione isolation result. (In all these calculations, α_{EM} was set to $1/137$, for the reasons noted above.)

The results of the comparison are shown in figs. 3 and 4 as a function of the photon p_T . Fig. 3 shows the CMS measurement, with its statistical and systematic uncertainties, along with the NLO predictions for a fixed-cone isolation as given using JETPHOX in ref. [14], and for the Frixione isolation criterion computed using the Gordon–Vogelsang code. The scale variation band shown was computed using JETPHOX. Fig. 4 compares several different NLO predictions to the JETPHOX prediction as given in ref. [14]: fixed-cone and Frixione isolation ones, using the Gordon–Vogelsang code, and one for the Frixione isolation, using BLACKHAT with SHERPA. All the predictions here use the CT10 parton distributions [32], which have $\alpha_s(M_Z) = 0.1179$. We see that the fixed-cone prediction from the Gordon–Vogelsang code, while not identical to the JETPHOX one, is in excellent agreement, well within the

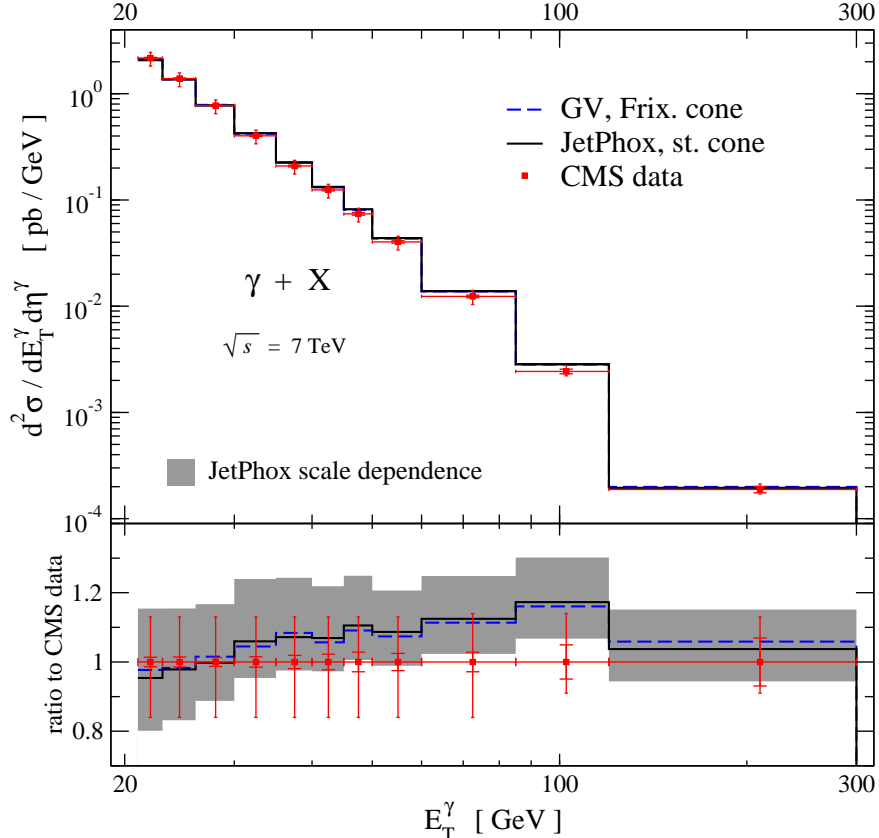


FIG. 3: A comparison of different NLO theoretical predictions for $\gamma + X$ production at the LHC at 7 TeV. The CMS data points [14] are shown (red) with combined experimental uncertainties; the prediction using the Gordon-Vogelsang (GV) code and the Frixione isolation criterion is given by the dashed (blue) line; the JETPHOX prediction using a standard cone isolation is given by the solid (black) line. The lower panel shows the two theoretical predictions normalized to the CMS data along with the scale dependence (shaded gray) as determined using JETPHOX.

experimental systematic uncertainties. In addition, the predictions for the Frixione-style isolation are also quite close, within 2% at low p_T^γ , and within 1% at high p_T^γ . It is the large- p_T region that is relevant to the primary study we perform in this paper. We expect that the smallness of this difference will carry over to processes with multiple jets in addition to the photon present here. We will include this difference in our overall uncertainty estimate for the Z -to-photon ratios. (See ref. [33] for a preliminary comparison between the two isolation criteria in the context of polarized pp scattering.) Fig. 4 also verifies the agreement in results from the Gordon–Vogelsang code for the Frixione-style isolation with those from BLACK-

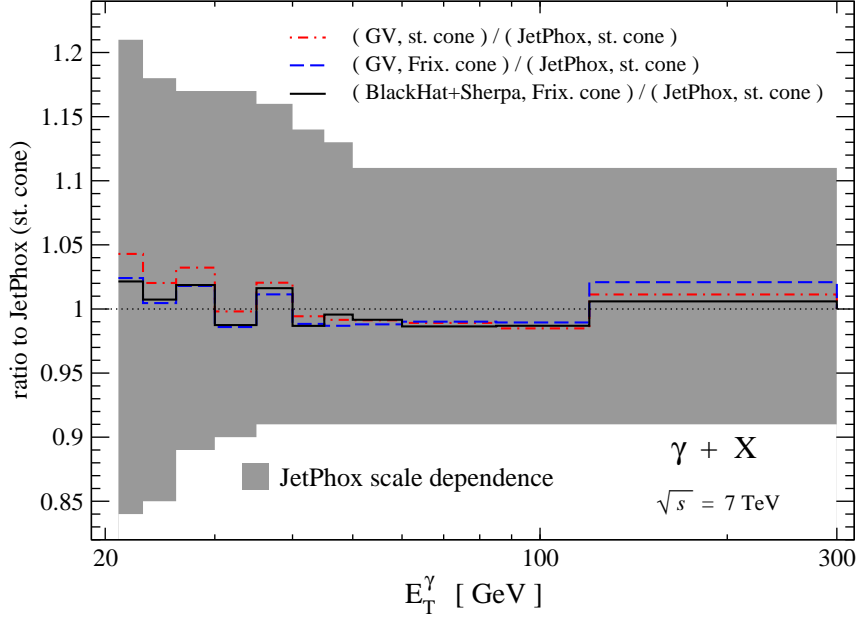


FIG. 4: A comparison of four different NLO predictions for $\gamma + X$ production at the LHC at 7 TeV. All predictions are normalized to the JETPHOX predictions shown in fig. 3. The prediction for a standard cone isolation using the Gordon-Vogelsang (GV) code is given by the dot-dashed (red) line; that for the Frixione isolation criterion using the GV code, by the dashed (blue) line; and that for the Frixione isolation using the BlackHat+Sherpa code, by the solid (black) line. The JETPHOX scale dependence band is shown in gray.

HAT+SHERPA to within 1%, uniformly in p_T^γ . In this particular BLACKHAT+SHERPA calculation, we impose no jet requirements, and impose a fixed maximum hadronic energy of 5 GeV in the isolation definition (2.3) in place of $E_T^\gamma \epsilon$ with $\epsilon = 0.025$ as done elsewhere in our $\gamma + 2$ -jet study. (The difference in cross sections between using a fixed energy of 5 GeV and the energy fraction used in our study is less than 1% for $p_T^\gamma > 50$ GeV.)

The rest of our study makes use of the MSTW08 parton distributions. Predictions with this set, which has a larger $\alpha_s(M_Z)$ of 0.1201, are 4% higher than those shown in fig. 3, fairly uniformly in p_T^γ ; however, this difference is expected to become much smaller when taking the ratio of $Z + 2$ - to $\gamma + 2$ -jet quantities.

IV. PHOTON-TO-Z RATIOS AT THE LHC

Our focus in this paper is on using distributions measured for $\gamma + 2$ -jet production to predict similar distributions assembled from missing $E_T + 2$ -jet events. Ideally, we would compute the ratio of fully-differential cross sections,

$$\frac{d\sigma^Z/dA}{d\sigma^\gamma/dA}, \quad (4.1)$$

where

$$\frac{d\sigma^V}{dA} \equiv \frac{d\sigma^{V+2\text{jets}}}{dE_T^{1\text{st jet}} d\eta^{1\text{st jet}} d\phi^{1\text{st jet}} dE_T^{2\text{nd jet}} d\eta^{2\text{nd jet}} d\phi^{2\text{nd jet}}}. \quad (4.2)$$

This information could be used experimentally by adjusting the weight of each $\gamma + 2$ jet event, removing the photon, and then reweighting the sample to obtain unit-weight events. This would provide a sample of estimated $Z + 2$ jet events with the Z decaying invisibly.

With sufficient statistics we could effectively construct such a quantity using n -tuples, tracking the matrix-element weights and parton momenta. However, besides the practical issue of carrying out such a procedure at NLO, we would have no way to usefully present such a quantity in two-dimensional form. Accordingly, we will study the ratios of a variety of singly-differential distributions. This can be thought of as a projected version of the above ratio, with a projection onto one of the axes in the complete differential cross section.

We use the anti- k_T jet algorithm [28] with clustering parameter $R = 0.5$, where $R = \sqrt{(\Delta y)^2 + (\Delta\phi)^2}$ as usual in terms of rapidity and azimuthal angle.

Our Monte Carlo set up allows us to study any infrared and collinear-safe observable. In the present study, we focus on three sets of cuts, theoretical parallels to those used by the CMS collaboration [1] and intended to be relevant in different regions of the SUSY parameter space. In order to display these cuts, we make use of a special definition of the total transverse energy, which we label H_T^{jet} , as the sum of the transverse energies of all jets with $p_T > 50$ GeV and $|\eta| < 2.5$. We also define a vector MET, as the negative of the sum of transverse momenta of all jets with $p_T > 30$ GeV and $|\eta| < 5$. Each set of cuts that we will consider is distinguished by different restrictions on the quantities¹ H_T^{jet} and MET.

Set 1: $H_T^{\text{jet}} > 300$ GeV, $|\text{MET}| > 250$ GeV,

¹ MET stands for ‘Missing Transverse Energy’. Although this is standard terminology, it is potentially misleading, as the MET is in fact the missing transverse momentum.

Set 2: $H_T^{\text{jet}} > 500$ GeV, $|\text{MET}| > 150$ GeV,

Set 3: $H_T^{\text{jet}} > 300$ GeV, $|\text{MET}| > 150$ GeV.

For all sets we insist that the two highest- p_T jets have p_T at least 50 GeV and pseudorapidity of at most $|\eta| = 2.5$. These jets are referred to as ‘tagging jets’. We note that beyond leading order there can be other jets in the event. The separation in ϕ -space between each tagging jet and the MET vector is required to satisfy $\Delta\phi(\text{jet}, \text{MET}) > 0.5$.

In addition to the above cuts, for the $\gamma + 2$ jet study only, we impose photon isolation according to the Frixione [12] prescription, with parameters $\epsilon = 0.025$, $\delta_0 = 0.3$ and $n = 2$, and a minimum R -space separation between the MET vector and each tagging jet of 0.4. The photon is required to have $|\eta| < 2.5$. We also impose a minimum p_T of 100 GeV on both the photon and the Z . This cut has no effect because of the $|\text{MET}|$ cut, but it improves the numerical efficiency of the calculation.

The Set 1 cuts can be roughly characterized as the low- H_T^{jet} / high-MET region, whereas Set 2 is the converse, high- H_T^{jet} / low-MET. The reason for studying these two sets is that different SUSY production mechanisms are expected to lead to signals in different regions. Broadly speaking, Set 1 is geared towards catching direct squark decays, while Set 2 is designed for cascades with a W -boson and a softer lightest supersymmetric particle (LSP). Set 3, which is inclusive of both the others, is a control region.

Our fixed-order results depend on the renormalization and factorization scales. These scales are unphysical, but necessarily appear when the perturbative series is truncated at a finite order. For fixed-order predictions, it is customary to estimate the error arising from omission of higher-order terms by varying these scales around some central value. The size of the resulting band is a useful diagnostic for those situations where fixed-order perturbation theory breaks down. The central value should be a typical hard scale in the process, to minimize the impact of potentially large logarithms. We choose the dynamical scale $\mu = H'_T/2$ for this central value, where H'_T is defined as

$$H'_T = \sum_i E_T^i + E_T(Z, \gamma), \quad (4.3)$$

where i runs over the partons and $E_T \equiv \sqrt{M^2 + p_T^2}$. A common method for estimating the error on a cross section is by varying the common scale up and down by a factor of two. We do so by evaluating the cross sections at five scales: $\mu/2, \mu/\sqrt{2}, \mu, \sqrt{2}\mu, 2\mu$. As we

process	LO	ME+PS	NLO
$Z + 2j$	$0.521(0.001)_{-0.125}^{+0.180}$	$0.416(0.004)$	$0.560(0.002)_{-0.042}^{+0.012}$
$\gamma + 2j$	$2.087(0.005)_{-0.494}^{+0.716}$	$1.943(0.027)$	$2.448(0.008)_{-0.225}^{+0.142}$
Z/γ ratio	0.250	0.214	0.229

TABLE I: Set 1 cross sections for Z and γ production in association with two jets, using the anti- k_T jet algorithm. The numbers in parentheses are Monte Carlo statistical errors, while the upper and lower limits represent scale dependence. See the text for a discussion of the errors on the ratio.

process	LO	ME+PS	NLO
$Z + 2j$	$0.205(0.001)_{-0.050}^{+0.073}$	$0.238(0.005)$	$0.277(0.002)_{-0.033}^{+0.032}$
$\gamma + 2j$	$0.952(0.004)_{-0.230}^{+0.333}$	$1.132(0.010)$	$1.374(0.008)_{-0.148}^{+0.268}$
Z/γ ratio	0.215	0.211	0.201

TABLE II: As in Table 1, but for the Set 2 cuts.

will discuss below, this procedure is expected to greatly underestimate uncertainties when applied to a ratio of cross sections.

V. LHC PREDICTIONS

In this section we present total cross sections and distributions for $\gamma + 2$ -jet and $Z + 2$ -jet production at the LHC running at 7 TeV. We present results for each of the three sets of cuts. In the $Z + 2$ jet study we fold in the Z boson decay into neutrinos, which comprise the missing energy. The branching ratio for the Z to decay to neutrinos is largely responsible for the $\gamma + 2$ jets cross section being about a factor of five larger than for $Z(\rightarrow \nu\bar{\nu}) + 2$ jets. This ratio is clearly visible in our figures, and is of course the underlying motivation for this study. We will also discuss the error to be assigned to our predictions.

In Tables I, II and III we give the total cross section for the cuts outlined in the previous section. Each table shows three different theoretical predictions. Fixed-order perturbative results are shown as LO and NLO. The final states in these cases consist of the vector boson with the two tagging jets, though there can be an extra jet at NLO. The parton shower result,

process	LO	ME+PS	NLO
$Z + 2j$	$1.255(0.002)^{+0.429}_{-0.296}$	1.174(0.011)	$1.476(0.007)^{+0.090}_{-0.136}$
$\gamma + 2j$	$5.854(0.011)^{+1.975}_{-1.361}$	6.075(0.056)	$7.601(0.019)^{+0.754}_{-0.826}$
Z/γ ratio	0.215	0.194	0.195

TABLE III: As in Table 1, but for the Set 3 cuts.

labeled “ME+PS”, is a tree-level matrix element calculation merged to a parton shower [11], as summarized above. Here the final state can contain many jets, though virtual corrections are not taken into account. The LO predictions are the least reliable of the three and are shown only for reference purposes.

With the cuts of Sets 1 and 2, the corrections from LO to NLO lead to an increase in the total cross sections of up to 50%. The corrections for the control region, given by the Set 3 cuts, are much more modest. The ME+PS and NLO results do not agree well for the cross sections. However, when one takes the ratio of Z and γ cross sections, the two predictions agree to within better than 10%. This behavior is not surprising: typically, overall normalizations can be somewhat off in ME+PS calculations, while ratios tend to behave much better.

We have found that in the ratio the LO scale variation cancels nearly completely, if we vary the scale in a correlated way in the $Z + 2$ -jet and $\gamma + 2$ -jet predictions. In the NLO case the scale variation is a bit larger but also very small. This nearly complete cancellation of the scale variation cannot be interpreted as a small theoretical uncertainty. The closeness of the NLO and ME+PS ratios is a much better indication that the theoretical uncertainties on the individual cross sections do indeed largely cancel in the ratio. We do not include the uncertainty due to the parton distributions in our study, but we expect it to largely cancel in the ratio since the $d(x)/u(x)$ ratio feeding into it is from a well-measured region in x .

Let us turn next to an examination of five different distributions: the transverse momentum of the first (largest p_T) accompanying jet; the p_T of the second jet; the total transverse energy of the jets H_T^{jet} ; and the azimuthal angle distributions with respect to the MET vector of the first and second accompanying jets. These variables are useful for assessing the extent to which the kinematics of $\gamma + 2$ -jet events resembles that of $Z + 2$ -jet events.

The p_T distribution for the leading jet is shown in fig. 5. The peak in the distribution is

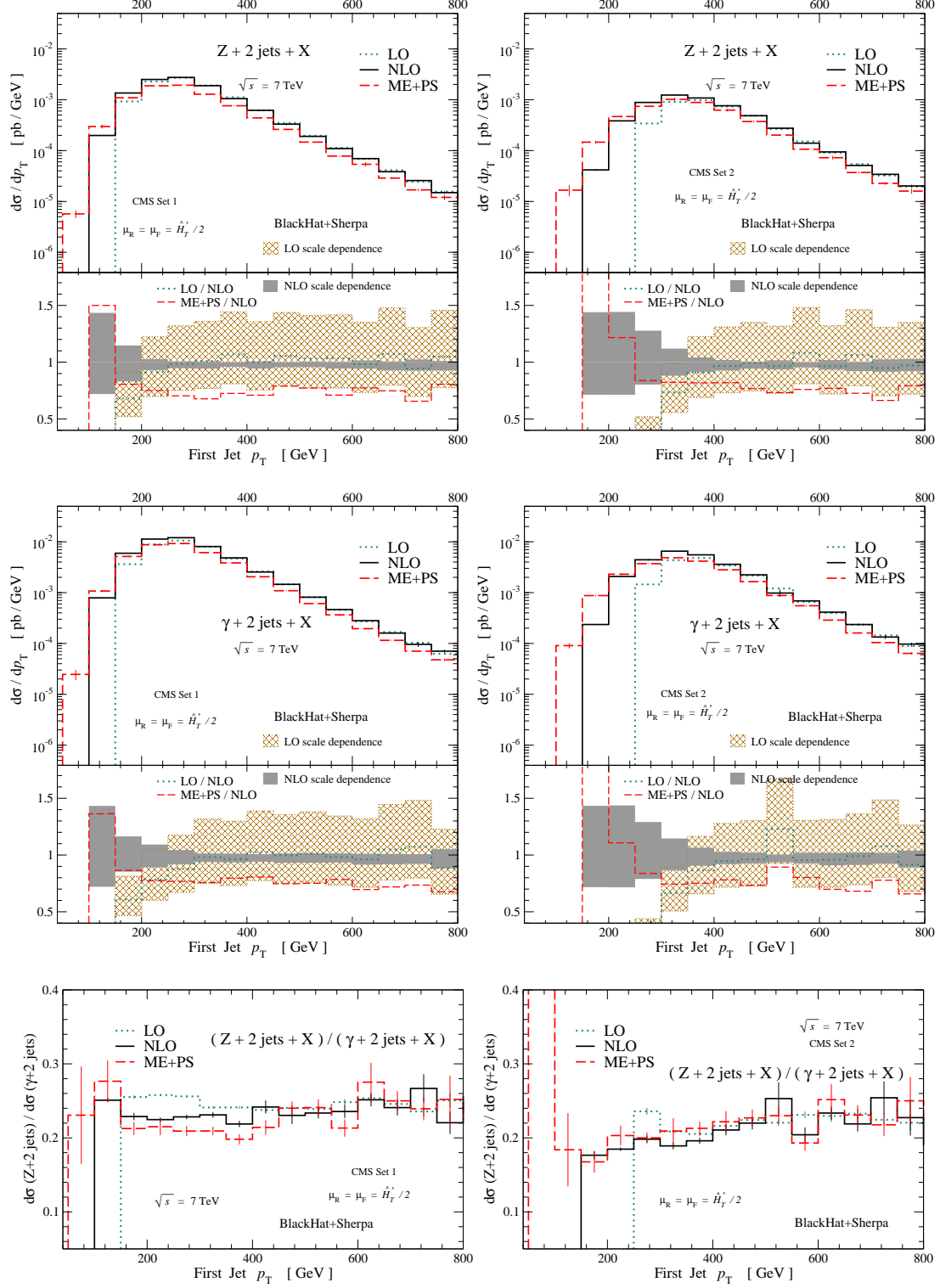


FIG. 5: The p_T distribution of the first jet. The left column shows distributions for the Set 1 cuts, and the right column for the Set 2 cuts. Each column displays the differential cross section for $Z + 2$ -jet production (top), $\gamma + 2$ -jet production (middle), and their ratio (bottom). In the top and middle plots, the upper panel shows the LO, NLO, and ME+PS results for the distribution, and the lower panel shows the ratio to the central NLO prediction, along with the LO and NLO scale-dependence bands. The numerical integration uncertainties are indicated by thin vertical lines.

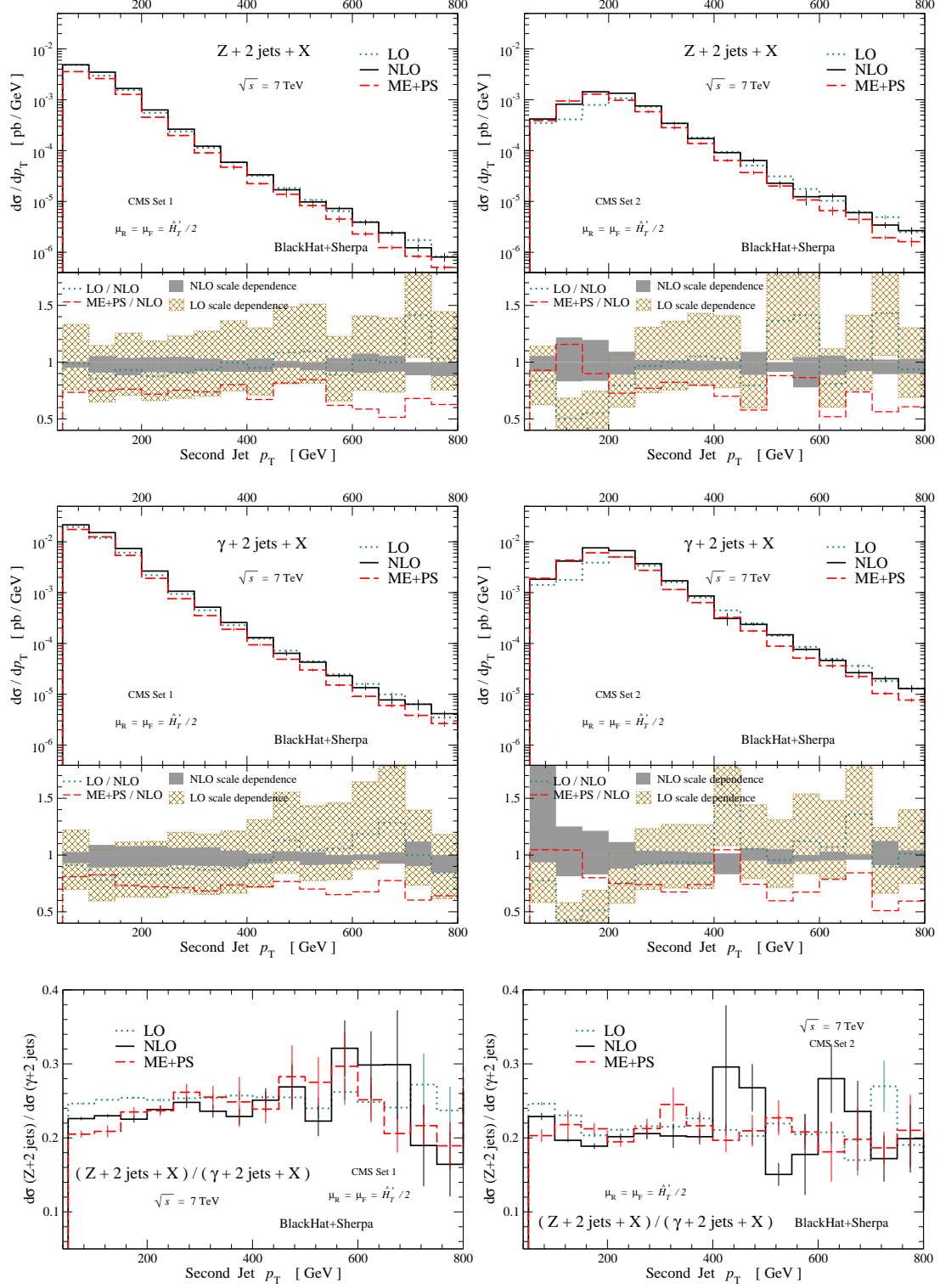


FIG. 6: The p_T distribution of the second jet. The plots are arranged and the curves are labeled as in fig. 5.

well above the jet cut, because of the additional cuts on the MET and H_T^{jet} . The LO cross

section vanishes below 150 GeV for Set 1 and 250 GeV for Set 2, due to the restricted LO kinematics, which are relieved both at NLO, from the presence of one additional parton, or in the ME+PS approximation, which can have several additional partons (including the parton shower). Clearly fixed-order LO is inadequate for describing the p_T distribution for the leading jet.

The p_T distribution for the second accompanying jet is shown in fig. 6; we consider only $p_T > 50$ GeV. This distribution is peaked at the jet cut of 50 GeV for Set 1, and falls rapidly with increasing p_T . For Set 2, in contrast, the distribution peaks at a second-jet p_T of around 180 GeV. The latter reflects a compensation for the higher total jet E_T needed to arrive at the minimum H_T^{jet} in this set; a second jet at the lower cut would force the leading jet too far out onto the tail of its distribution. The NLO corrections for Set 1 are approximately 20%, in line with the corrections to the total cross section. These corrections are roughly flat across the distribution, so that the shape does not change at NLO. The NLO corrections for Set 2, in contrast, are significantly larger, up to 100% in some bins of second-jet p_T , but under 10% for p_T above 300 GeV, but below 400 GeV, where the integration errors become large. The shape of the distribution correspondingly suffers significant corrections at NLO. For both sets, however, the corrections do not distinguish Z and γ production, so that the ratio has NLO corrections of 10–15%, but flat across all p_T s. The NLO and ME+PS results are likewise in good and uniform agreement for the ratio, to better than 10%, again ignoring regions with large integration errors. As expected, the scale-dependence bands, from varying the common renormalization and factorization scale, $\mu_R = \mu_F$, up and down by a factor of two, are narrower at NLO than at LO.

The situation changes slightly if we examine the H_T^{jet} distributions, shown in fig. 7. In both Sets 1 and 2, these are falling distributions which peak at the cut values for H_T^{jet} (300 and 500 GeV, respectively). In Set 1, the NLO corrections range from 10% to 50%, gradually increasing with increasing H_T^{jet} through 550 GeV or so; the shape of the distribution is thus modified at NLO. In contrast, the corrections for Set 2 are fairly uniform across all H_T^{jet} , presumably because of the larger H_T^{jet} starting scale for the distribution. Once again, the corrections do not distinguish between Z and γ production, so that the ratios for both Sets 1 and 2 have NLO corrections of about 10–15%, with corrections relatively flat across all H_T^{jet} . The NLO and ME+PS results for the ratio are again in good and uniform agreement, to better than 10%. In both sets, the scale-dependence bands are uniformly narrower at

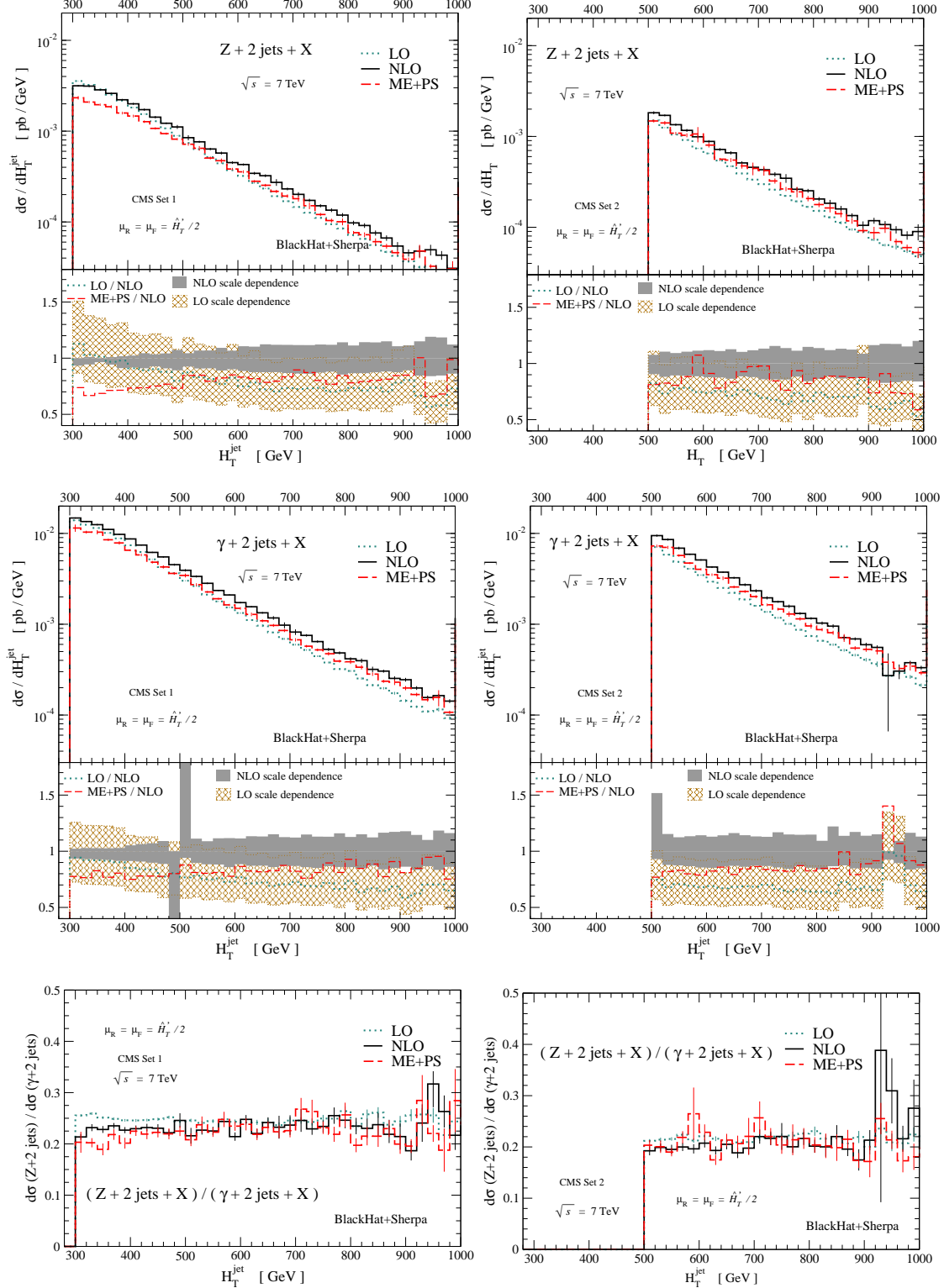


FIG. 7: The H_T^{jet} distribution. The left column shows distributions for the Set 1 cuts, and the right column for the Set 2 cuts. The plots are arranged and the curves are labeled as in figs. 5 and 6.

NLO than at LO.

The distributions which show the most structure are those in the azimuthal angle $\Delta\phi(\text{MET}, \text{jet}_i)$ between the MET vector and the two jets, shown in fig. 8. The distribution for the first jet is peaked near $\Delta\phi = \pi$, where the leading jet balances the MET vector while the second jet has much smaller p_T . The distribution falls very steeply at smaller angle. A typical LO configuration for the Set 1 cuts is shown in fig. 9(a). With only two partons and a missing energy vector from the Z or γ , transverse momentum conservation implies that the leading jet can never get closer in angle than $\pi/2$ to the MET vector. It can only approach this angle if the transverse momenta of both jets are extremely large. This configuration is heavily suppressed by the parton distributions, to orders of magnitude below what is shown in fig. 8. At NLO, this kinematic constraint is relaxed, as it is possible in the real-emission configurations for the second and third jets (the latter may fall below the jet p_T threshold) to balance the leading jet and MET vector, as shown schematically in fig. 9(b). At this order, the leading-jet distribution does indeed run all the way to the $\Delta\phi(\text{MET}, \text{jet}) = 0.5$ cut we impose. The cross section for angles less than $\pi/2$ is tiny, however, so although the NLO corrections are very large in this region, they are of no practical importance; this carries over to the large corrections seen in the ratio of $Z + 2\text{-jet}$ and $\gamma + 2\text{-jet}$ distributions.

The width of the peak region in the $\Delta\phi$ distribution for the leading jet can be understood by considering a configuration in which the second jet has $p_T \simeq 50$ GeV and 180 GeV for Sets 1 and 2 respectively, with the leading jet having the minimum p_T needed to balance the MET given a jet–jet $\Delta\phi = 0.5$ (the interjet ΔR cut). This would lead to a peak around $\Delta\phi \simeq 3.05$ for Set 1, and 3.0 for Set 2. However, the shapes of the ratios of distributions do differ somewhat between the NLO and ME+PS predictions for the peak region of the Set 1 distribution ($\Delta\phi \sim 2.8\text{--}3.0$), so that the analysis would be more sensitive to any systematic effects in the treatment of this region.

In the $\Delta\phi$ distribution for the second jet, we see different structure in the small-angle region for $Z + 2\text{-jet}$ and $\gamma + 2\text{-jet}$ production. For Set 1, this region is subdominant in its contributions, although not completely negligible, because the high MET cut favors configurations in which both jet transverse momenta oppose the MET vector, as shown in fig. 9(a). In Set 2, however, the low MET cut allows small values of $\Delta\phi(\text{MET}, \text{jet}_2)$ to dominate. In this region, the potential collinear singularity between a photon and an outgoing quark forming the second jet causes the cross section to start to rise at small

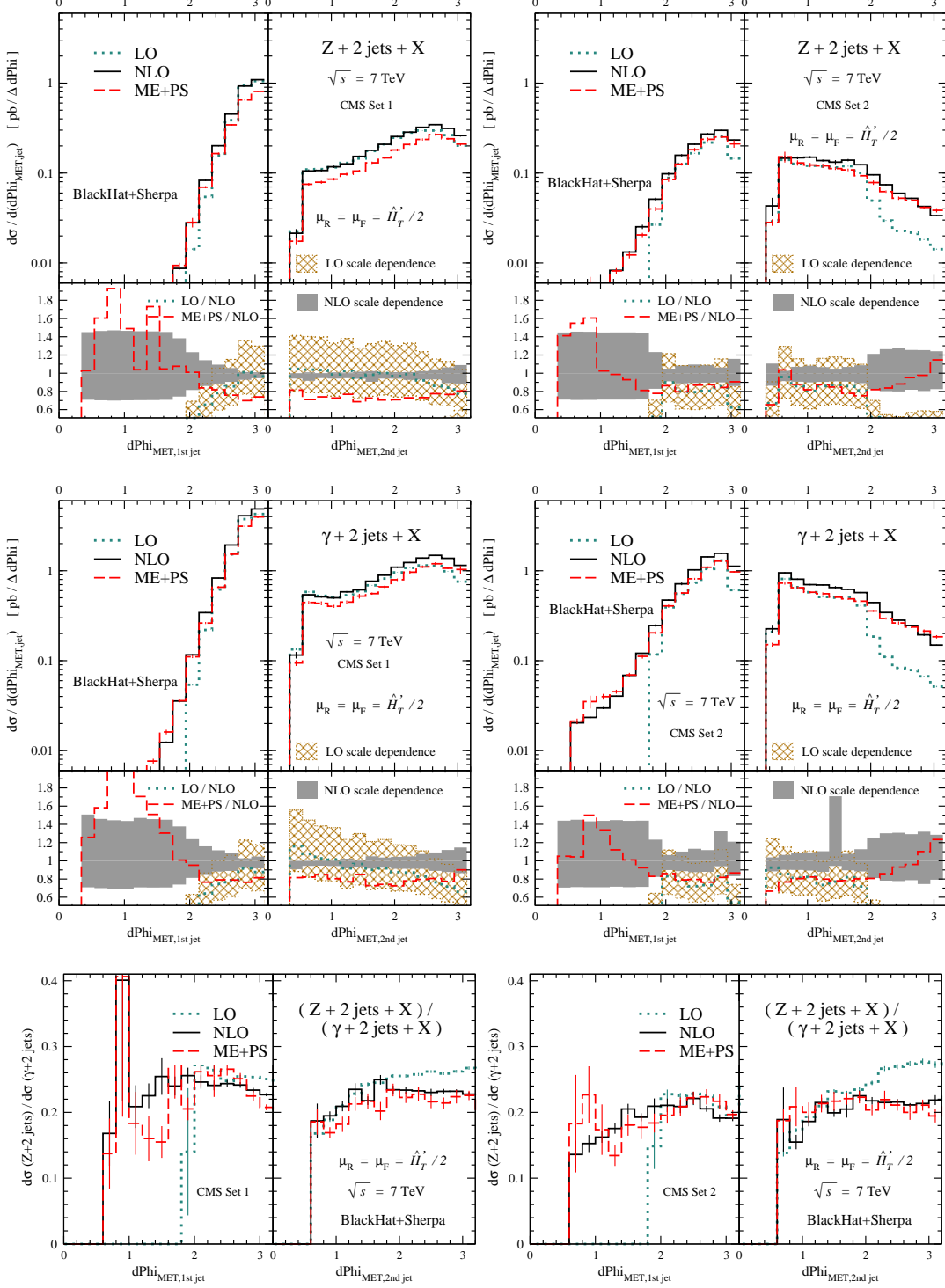


FIG. 8: The $\Delta\phi(\text{MET},\text{jet})$ distributions for the leading two jets. The left column shows the distributions for the Set 1 cuts, and the right column for the Set 2 cuts. Each column displays the differential cross section for $Z + 2$ -jet production (top), $\gamma + 2$ -jet production (middle), and their ratio (bottom). The left panel of each plot shows the distribution for the leading jet, and the right panel for the second jet. In the top and middle plots, the upper panel shows the LO, NLO, and ME+PS results for the distribution, and the lower panel shows the ratio to the central NLO prediction, along with the LO and NLO scale-dependence bands.

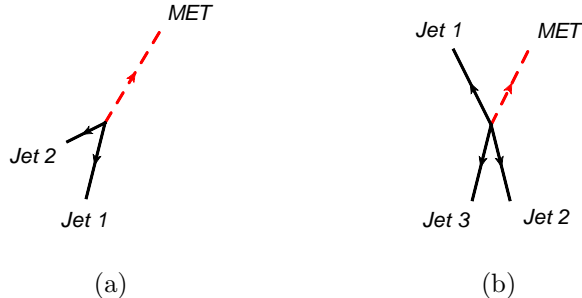


FIG. 9: A typical configuration of jets and MET vector for the Set 1 cuts at (a) LO and (b) NLO.

angles. This rise is cut off by the $\Delta\phi(\text{MET}, \text{jet})$ cut, but does distinguish Z production from photon production. For both Sets 1 and 2, the shapes of the ratios of distributions are similar at LO, at NLO, and in the ME+PS results, so that we can be confident the Z -to- γ difference is captured properly, and that the analysis should not be overly sensitive to the precise value chosen for the $\Delta\phi(\text{MET}, \text{jet})$ cut. The shapes of the NLO and ME+PS distributions (though not the LO one) are quite similar as well in the peak region, so that the analysis should be robust under systematic effects treating different angular regions in $\Delta\phi(\text{MET}, \text{jet}_2)$ somewhat differently.

To assess the overall uncertainty, we see that the ME+PS prediction for the total cross section with the Set 1 cuts is approximately 7% lower than the NLO prediction, while for the Set 2 cuts it is approximately 5% higher. In addition, we should allow for a difference of up to 1% in the prediction for the fixed-cone isolation compared to the Frixione-style isolation, as discussed in section III. This suggests that the NLO predictions for the ratios used by the CMS collaboration should be accurate to within 10%.

We have not considered the effect of possible electroweak Sudakov logarithms. Based on refs. [34], we estimate that for Set 1, the effect will be under 5% and smaller for Sets 2 and 3. Our study considers production of an (exclusive) electroweak boson accompanied by at least two jets rather than one; we expect the electroweak effects to be of similar magnitude for similar boson transverse momenta. If one were to raise the MET cut, these electroweak corrections increase, and would need to be taken into account to ensure the reliability of the prediction for the $Z + 2\text{-jet}$ to $\gamma + 2\text{-jet}$ ratio. Were the MET cut to be raised to 500 GeV, for example, the virtual electroweak corrections would grow to about 10%. The effects of radiating a second electroweak gauge boson into the final state [35] should also be

considered. These questions merit further investigation.

VI. CONCLUSIONS AND OUTLOOK

Data-driven estimates of backgrounds to new physics signals offer a powerful means for avoiding a reliance on Monte Carlo estimates of backgrounds. Even in such data-driven methods, theoretical input is usually required to provide conversion factors from one process to another, and estimates of uncertainties in these factors, as well as of extrapolations from control to signal regions.

In this paper, we studied the theoretical aspects of using γ +jets data to estimate the missing- E_T + jets background to new-physics searches. We focused on the comparison of boson production in association with two or more jets, computing the relevant differential cross sections and ratios in NLO QCD. Because the scale uncertainty is quite small in these ratios, we used the difference between ME+PS results and the NLO ones as an estimate of theoretical uncertainty. (We did not study the uncertainty due to parton distribution functions, but it is expected to be small as well.) Our study used the Frixione isolation criterion to compute the prompt-photon cross sections; a comparison with the fixed-cone isolation for isolated prompt-photon production indicates that the resulting shift should be less than 1% in the high- p_T^γ region of interest. We did not include the effects of electroweak Sudakov logarithms, and while these will become significant for higher MET cuts, we expect the effects to remain small for the cuts used in this study.

We find that the conversion between photons and Z bosons has less than a 10% theoretical uncertainty for events with two associated jets. In the future, it should be feasible to extend this study to three associated jets. The small uncertainty we find should make it possible for the photon channel to provide a competitive determination of the Standard-Model missing- E_T + jets background for many years to come.

Note added

Since the appearance of our paper, CMS presented a new physics search based on an event signature of at least three jets accompanied by large missing transverse momentum [36]. No excess events were observed above the background. The irreducible background from Z bosons decaying into a $\nu\bar{\nu}$ pair was estimated by converting a measurement of photons accompanied by jets into a prediction of this background. Our paper provided the estimate

of the theoretical uncertainty for this conversion.

Acknowledgments

We thank Joe Incandela, Sue-Ann Koay, Steven Lowette, Roberto Rossin, Piet Verwilligen and Mariarosaria D’Alfonso, for suggesting this analysis, for bringing CMS’s study to our attention, and for extensive discussions. We thank André David and David d’Enterra for providing the JETPHOX predictions in ref. [14]. We thank Werner Vogelsang for providing a copy of his NLO isolated prompt-photon code, and Jean-Philippe Guillet for providing a copy of the JETPHOX code, and for discussions pertaining to it. We also thank Ed Berger, Thomas Gehrmann, Bernd Kniehl, Bill Marciano, Michael Peskin, Joe Polchinski, Alberto Sirlin and Bennie Ward for helpful discussions. We especially thank Carola Berger and Tanju Gleisberg for their contributions during early stages of this work. This manuscript was completed during a visit to the Kavli Institute for Theoretical Physics, and we thank it for its hospitality. This research was supported by the National Science Foundation under Grant No. NSF PHY05–51164, and by the US Department of Energy under contracts DE–FG03–91ER40662, DE–AC02–76SF00515 and DE–FC02–94ER40818. DAK’s research is supported by the European Research Council under Advanced Investigator Grant ERC–AdG–228301. This research used resources of Academic Technology Services at UCLA and of the National Energy Research Scientific Computing Center, which is supported by the Office of Science of the U.S. Department of Energy under Contract No. DE–AC02–05CH11231.

-
- [1] CMS Collaboration, “*Data-Driven Estimation of the Invisible Z Background to the SUSY MET Plus Jets Search*”, CMS PAS SUS-08-002 (2008), unpublished.
 - [2] CMS Collaboration, “*Search for new Physics at CMS with Jets and Missing Momentum*”, CMS PAS SUS-10-005 (2010), unpublished.
 - [3] C. F. Berger, Z. Bern, L. J. Dixon, F. Febres Cordero, D. Forde, T. Gleisberg, H. Ita, D. A. Kosower and D. Maître, Phys. Rev. D **80**, 074036 (2009) [0907.1984 [hep-ph]].
 - [4] C. F. Berger, Z. Bern, L. J. Dixon, F. Febres Cordero, D. Forde, T. Gleisberg, H. Ita, D. A. Kosower and D. Maître, Phys. Rev. Lett. **106**, 092001 (2011) [1009.2338 [hep-ph]].

- [5] C. F. Berger, Z. Bern, L. J. Dixon, F. Febres Cordero, D. Forde, T. Gleisberg, H. Ita, D. A. Kosower and D. Maître, Phys. Rev. D **82**, 074002 (2010) [1004.1659 [hep-ph]].
- [6] Z. Bern, G. Diana, L. J. Dixon, F. Febres Cordero, D. Forde, T. Gleisberg, S. Höche, H. Ita, D. A. Kosower, D. Maître and K. Ozeren, 1103.5445 [hep-ph].
- [7] C. F. Berger, Z. Bern, L. J. Dixon, F. Febres Cordero, D. Forde, H. Ita, D. A. Kosower and D. Maître, Phys. Rev. D **78**, 036003 (2008) [0803.4180 [hep-ph]].
- [8] C. F. Berger, Z. Bern, L. J. Dixon, F. Febres Cordero, D. Forde, T. Gleisberg, H. Ita, D. A. Kosower and D. Maître, Phys. Rev. Lett. **102**, 222001 (2009) [0902.2760 [hep-ph]].
- [9] F. Krauss, R. Kuhn and G. Soff, JHEP **0202**, 044 (2002) [hep-ph/0109036];
T. Gleisberg and F. Krauss, Eur. Phys. J. C **53**, 501 (2008) [0709.2881 [hep-ph]].
- [10] T. Gleisberg, S. Höche, F. Krauss, A. Schalicke, S. Schumann and J. C. Winter, JHEP **0402**, 056 (2004) [hep-ph/0311263];
T. Gleisberg, S. Höche, F. Krauss, M. Schönherr, S. Schumann, F. Siegert and J. Winter, JHEP **0902**, 007 (2009) [0811.4622 [hep-ph]].
- [11] S. Höche, S. Schumann and F. Siegert, Phys. Rev. D **81**, 034026 (2010) [0912.3501 [hep-ph]].
- [12] S. Frixione, Phys. Lett. B **429**, 369 (1998) [hep-ph/9801442].
- [13] L. Bourhis, M. Fontannaz and J. P. Guillet, Eur. Phys. J. C **2**, 529 (1998) [hep-ph/9704447].
- [14] V. Khachatryan *et al.* [CMS Collaboration], Phys. Rev. Lett. **106**, 082001 (2011) [1012.0799 [hep-ex]].
- [15] S. Catani and M. H. Seymour, Nucl. Phys. B **485**, 291 (1997) [Erratum-ibid. B **510**, 503 (1998)] [hep-ph/9605323].
- [16] Z. Bern, L. J. Dixon and D. A. Kosower, Nucl. Phys. B **513**, 3 (1998) [hep-ph/9708239].
- [17] Z. Bern, L. J. Dixon, D. A. Kosower and S. Weinzierl, Nucl. Phys. B **489**, 3 (1997) [hep-ph/9610370].
- [18] J. M. Campbell, E. W. N. Glover and D. J. Miller, Phys. Lett. B **409**, 503 (1997) [hep-ph/9706297].
- [19] Z. Bern, L. J. Dixon and D. A. Kosower, Nucl. Phys. B **437**, 259 (1995) [hep-ph/9409393].
- [20] Z. Kunszt, A. Signer and Z. Trócsányi, Phys. Lett. B **336**, 529-536 (1994) [hep-ph/9405386].
- [21] A. Signer, Phys. Lett. B **357**, 204 (1995) [hep-ph/9507442].
- [22] J. M. Campbell and R. K. Ellis, Phys. Rev. D **65**, 113007 (2002) [hep-ph/0202176].
- [23] T. Gleisberg and S. Höche, JHEP **0812**, 039 (2008) [0808.3674 [hep-ph]].

- [24] S. Schumann and F. Krauss, JHEP **0803**, 038 (2008) [0709.1027 [hep-ph]].
- [25] S. Höche, S. Schumann and F. Siegert, Phys. Rev. D **81**, 034026 (2010) [0912.3501 [hep-ph]].
- [26] B. A. Kniehl and L. Lönnblad, DESY 92-032 (1992), in *Proceedings of the Annecy Photon Workshop (1991)*.
- [27] A. Czarnecki and W. J. Marciano, Phys. Rev. Lett. **81**, 277 (1998) [hep-ph/9804252].
- [28] M. Cacciari, G. P. Salam and G. Soyez, JHEP **0804**, 063 (2008) [0802.1189 [hep-ph]].
- [29] J. R. Andersen *et al.* [SM and NLO Multileg Working Group], 1003.1241 [hep-ph] (page 94).
- [30] S. Catani, M. Fontannaz, J. Ph. Guillet and E. Pilon, JHEP **0205**, 028 (2002) [hep-ph/0204023];
P. Aurenche, M. Fontannaz, J. Ph. Guillet, E. Pilon and M. Werlen, Phys. Rev. D **73**, 094007 (2006) [hep-ph/0602133].
- [31] L. E. Gordon and W. Vogelsang, Phys. Rev. D **50**, 1901 (1994).
- [32] H.-L. Lai, M. Guzzi, J. Huston, Z. Li, P. M. Nadolsky, J. Pumplin and C.-P. Yuan, Phys. Rev. D **82**, 074024 (2010) [1007.2241 [hep-ph]].
- [33] S. Frixione and W. Vogelsang, Nucl. Phys. B **568**, 60 (2000) [hep-ph/9908387].
- [34] E. Maina, S. Moretti and D. A. Ross, Phys. Lett. B **593**, 143 (2004) [Erratum-ibid. B **614**, 216 (2005)], [hep-ph/0403050];
J. H. Kuhn, A. Kulesza, S. Pozzorini and M. Schulze, JHEP **0603**, 059 (2006) [hep-ph/0508253].
- [35] U. Baur, Phys. Rev. D **75**, 013005 (2007) [hep-ph/0611241].
- [36] S. Chatrchyan *et al.* [CMS Collaboration], 1106.4503 [hep-ex].